JARO 17: 159–171 (2016)
DOI: 10.1007/s10162-016-0562-z
© 2016 Association for Research in Otolaryngology

JARO
Journal of the Association for Research in Otolaryngology

Research Article

Scanning Electron Microscopic Examination of the Extracellular Matrix in the Decellularized Mouse and Human Cochlea

Peter A. Santi,[1] Robair Aldaya,[1] Alec Brown,[1] Shane Johnson,[1] Tyler Stromback,[1] Sebahattin Cureoglu,[1] and Helge Rask-Andersen[2]

[1]*Department of Otolaryngology, University of Minnesota, Lions Research Building 2001 Sixth Street, SE, Minneapolis, MN 55455, USA*

[2]*Department of Surgical Sciences, Head and Neck Surgery, Section of Otolaryngology, Uppsala University Hospital, 751 85, Uppsala, Sweden*

Received: 10 December 2015; Accepted: 15 March 2016; Online publication: 30 March 2016

ABSTRACT

Decellularized tissues have been used to investigate the extracellular matrix (ECM) in a number of different tissues and species. Santi and Johnson JARO 14:3-15 (2013) first described the decellularized inner ear in the mouse, rat, and human using scanning thin-sheet laser imaging microscopy (sTSLIM). The purpose of the present investigation is to examine decellularized cochleas in the mouse and human at higher resolution using scanning electron microscopy (SEM). Fresh cochleas were harvested and decellularized using detergent extraction methods. Following decellularization, the ECM of the bone, basilar membrane, spiral limbus, and ligament remained, and all of the cells were removed from the cochlea. A number of similarities and differences in the ECM of the mouse and human were observed. A novel, spirally directed structure was present on the basilar membrane and is located at the border between Hensen and Boettcher cells. These septa-like structures formed a single row in the mouse and multiple rows in the human. The basal lamina of the stria vascularis capillaries was present and appeared thicker in the human compared with the mouse. In the mouse, numerous openings beneath the spiral prominence that previously housed the root processes of the external sulcus cells were observed but in the human there was only a single row of openings. These and other anatomical differences in the ECM between the mouse and human may reflect functional differences and/or be due to aging; however, decellularized cochleas provide a new way to examine the cochlear ECM and reveal new observations.

Keywords: cochlea, SEM, decellularized, mouse, human

INTRODUCTION

Transmission and scanning electron microscopic images of normal and damaged cochleas have been reported for many years (Engstrom 1951; Smith and Sjoestrand 1961; Friedmann 1962; Duvall et al. 1966; Iurato 1967; Lim 1969; 1970) among others. From these studies, the anatomical features of the cochlea in a variety of species and in the human have been established. However, our understanding of cochlear morphology has been derived primarily from fixed and histologically processed tissue that contains numerous artifacts that result during chemical fixation, dehydration, and embedding. When tissues are processed by different histological methods, new anatomical structures may be revealed and change our understanding of cochlear anatomy. A classic example was the early fixation of the cochlea by osmium tetroxide for TEM and the seemingly empty nature of the cytoplasm of Claudius cells.

Correspondence to: Peter A. Santi · Department of Otolaryngology · University of Minnesota · Lions Research Building 2001 Sixth Street, SE, Minneapolis, MN 55455, USA. Telephone: 612-626-9881; email: psanti@umn.edu

When tissues were fixed with a cross-linking fixative such as glutaraldehyde and then postfixed by osmium tetroxide, these cells were observed to contain abundant cytosol. In addition, some structures, such as the hydrated glycoproteins and glycosaminoglycans abundant in the acellular tectorial membrane, continue to elude visualization since they are either un-fixed or removed from the tissue during processing or dramatically shrink with tissue dehydration. Specialized methods such as Cuprolinic blue and tungsten preserve and reveal some carbohydrate residues, but in a collapsed state (Tsuprun and Santi 2001).

We (Tsuprun and Santi 1999) previously described the molecular composition and 3D organization of the ECM in the chinchilla. The spiral limbus, ligament, and basilar membrane demonstrated regional differences in molecular composition and structural organization of the ECM. Type II collagen is abundant in the spiral limbus and spiral ligament; whereas, fibronectin and tenascin are abundant in the homogenous matrix of the basilar membrane. Radial-directed bundles of collagen type II are also present in the basilar membrane. Basal lamina distribution in the cochlea was previously reported by Tsuprun and Santi (1999). Three types of basal lamina in the cochlea were described: epithelial, endothelial, and perineurial. A continuous epithelial basal lamina extended from the attachment of Reissner's membrane at the apex of the stria, across the columnar plates and interdental cells of the spiral limbus, along the basal border of the inner sulcus cells, along the basilar membrane beneath the organ of Corti, Boettcher and Claudius cells, up the basilar crest, along the root process of the external sulcus cells, and beneath the spiral prominence to end at the attachment of the stria vascularis. No basal lamina was present along the basal cells of the stria vascularis or the underlying spiral ligament. Basal lamina was present around the vessels including the capillaries of the stria vascularis and surrounding the nerves and cell bodies of the spiral ganglion neurons.

Santi and Johnson (2013) reported on the ECM of the cochlea and vestibular system after decellularization in mouse, rat, and human at the light microscopic level. Using a microtome/microscope called scanning thin-sheet laser imaging microscopy (sTSLIM), we examined complete serial sections (~300) of the cochlea. The most notable feature that was observed was a new structure on the apical surface of the basilar membrane. This structure was located at the border of Hensen and Boettcher cells and it appeared as a spirally directed, periodic structure with septa-like projections of the ECM from the basilar membrane. This structure disappeared toward the cochlear apex, which is similar to Boettcher cell distribution. In another publication, we (Liu et al. 2015) showed that this structure was immunopositive for laminin and type IV collagen, further supporting the role of this structure as a component of the ECM. This publication also presented preliminary SEM observations from one human decellularized cochlea in a single composite image. The purpose of the present study was to further investigate the anatomy of the mouse and human cochlear ECM following decellularization using a higher resolution method, namely, SEM.

METHODS

Fourteen healthy young C57BL/6 mice were used in this study. The mice were euthanized for another study, and their waste tissue, which included their cochleas, was harvested from their temporal bones and decellularized by two methods. Twelve cochleas were perfused with sodium dodecyl sulfate (SDS), and two cochleas were perfused with 1 % sodium deoxycholate (SDOC). Both the SDS and SDOC were used to lyse all the cells in fresh, unfixed cochleas in order to examine the ECM. Specifically, a polypropylene strand was used to open the round and oval window membranes, and the perilymphatic space was perfused with either detergent for 5 min. Cochleas were then immersed in the detergent for 2 days at 4° with continuous rotation. Cochleas were washed in phosphate-buffered saline (PBS) for 15 min and then perfused and fixed in an aqueous solution of 4 % paraformaldehyde (PFA) for 2 days. Cochleas were rinsed twice for 15 min in deionized water, and three cochleas (decellularized with SDS) were processed by the OTO method (Seligman et al. 1966), while the remaining cochleas were post-fixed only in 1 % osmium tetroxide for 1 h.

The OTO method involved immersing specimens in 1 % osmium tetroxide for 1 h, rinsing in deionized water for 15 min, immersion in fresh 1 % thiocarbohydrazide for 20 min, an additional rinse for 15 min in deionized water, and another immersion fixation in 1 % osmium tetroxide for 1 h. Following the OTO or paraformaldehyde/osmium tetroxide fixation, all tissue was rinsed twice in deionized water for 15 min and decalcified in a 10 % solution of the disodium salt of ethylenediaminetetraacetic acid (EDTA) for 6 days. Cochleas were then rinsed for 4 h in deionized water for three times, followed by 4 h of dehydration in 75 % ethanol. Cochleas were gently bisected with a razor blade and then immersed and dehydration in 100 % ethanol for 24 h. All dehydrated specimens were critical-point dried with carbon dioxide and coated with gold-palladium in a sputter coater.

Three human temporal bones were used in this study, and harvesting was approved by our Human Subjects Institutional Review Board (#0206 M26181). The humans were two females, one male ages 55, 63, and 67 years. The temporal bones were removed from the humans after death (two cardiac and one lymphoma), and the perilymphatic spaces of the cochlea were perfused for 5 min with sodium dodecyl sulfate (SDS). The SDS was used to lyse and remove all the cells in fresh, unfixed cochleas. Cochleas were immersed in SDS for 1 week at 4° with continuous rotation and then for 1 week at room temperature with rotation. Cochleas were washed in phosphate-buffered saline (PBS) for 15 min and then perfused and fixed in an aqueous solution of 10 % formalin for 2 days. Following fixation, tissue was rinsed twice in PBS for 2 h and decalcified in a 10 % solution of the disodium salt of ethylene-diaminetetraacetic acid (EDTA) for 60 days. Cochleas were rinsed for 4 h in PBS, followed by 2 days of dehydration in 50 and 70 % ethanol. Cochleas were bisected with a razor blade and decalcified in EDTA for an additional 2 days. Cochleas were dehydrated in 50, 70, and 100 % ethanol for 2 days in each solution. For sTSLIM imaging, cochleas were stained overnight in Rhodamine B in 100 % ethanol, rinsed with 100 % ethanol and cleared in 5:3 methyl salicylate benzyl benzoate for 4 days.

Cochleas were imaged by sTSLIM, and the clearing solution was removed by immersion in several changes of 100 % ethanol for 2 days. For SEM, cochleas were critical-point dried with carbon dioxide and coated with gold-palladium using a sputter coater. Cochleas were imaged using the Hitachi S3500N Variable Pressure Scanning Electron Microscope (SEM).

RESULTS

Mouse Cochlea

Since decellularization removes all of the cells of the cochlea, we used morphometric parameters to determine the location of certain structures in celllularized cochleas vs. decellularized cochleas. Figure 1a is an sTSLIM cross section through the scala media of a cellularized cochlea showing the width of the basilar membrane at 83 μm shown as "A." "B" measures 36 μm from the lateral edge of the basilar membrane to Boettcher cells, and "C" measures 47 μm from Boettcher cells to the medial edge of the basilar membrane. In Figure 1b, the same distances are 78, 32, and 43 μm, respectively, which are similar.

However, SEM flattens 3D structures into 2D images so distances in SEM are approximate, and tissues may shrink more after SEM vs. sTSLIM processing.

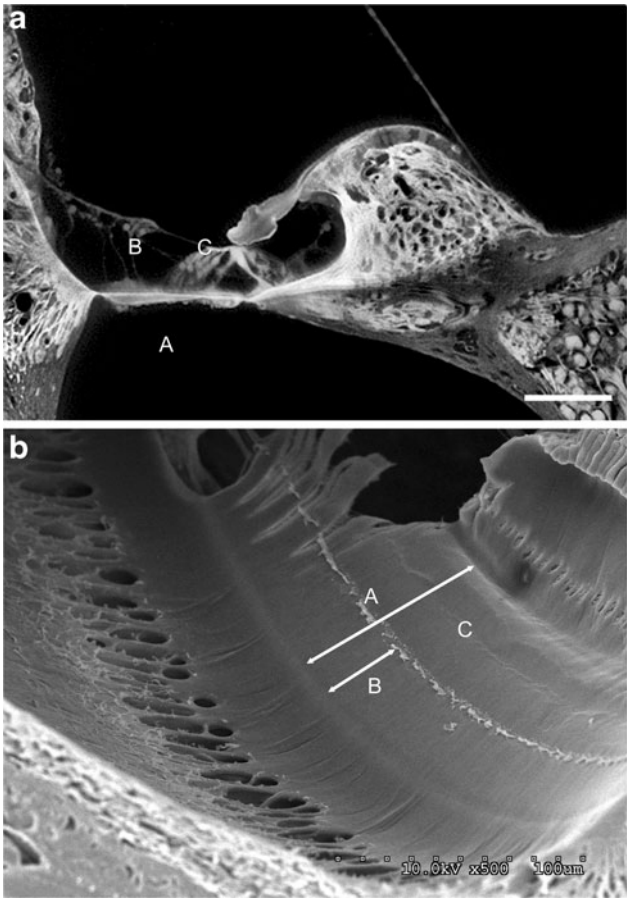

FIG. 1. **a** An sTSLIM cross section of the scala media from a cellularized mouse cochlea showing the basal turn. "*A*" marks the width of the basilar membrane (83 μm). "*B*" marks the distance (36 μm) from the lateral edge of the basilar membrane to the beginning of the Boettcher cells. "*C*" marks the distance (47 μm) from the medial edge of the basilar membrane to the beginning of Boettcher cells. *Bar* = 50 μm. **b** An SEM view of the scala media in a decellularized cochlea showing the basal turn. "*A*" marks the width 78 (μm) of the basilar membrane. "*B*" marks the distance (32 μm) from the lateral edge of the basilar membrane to the structure. "*C*" marks the distance (43 μm) from the structure to the medial edge of the basilar membrane. *Bar* = 100 μm.

SEM views of the decellularized cochlea confirmed our previous observations with sTSLIM (Santi and Johnson 2013), namely that a significant portion of the membranous labyrinth is composed of ECM. Figure 2 is an SEM "top-down" view of the basilar membrane looking from the scala vestibuli perspective. The lateral edge of spiral limbus appears as columnar plates of ECM. The habenula perforata are seen as a spirally directed, single line of openings beneath the spiral limbus. The basilar membrane surface is smooth from the habenula to the lateral wall except for an interruption by the newly described structure. In sTSLIM sections, this structure disappears at approximately 85–90 % of the distance from the base, and this distance corresponds to the

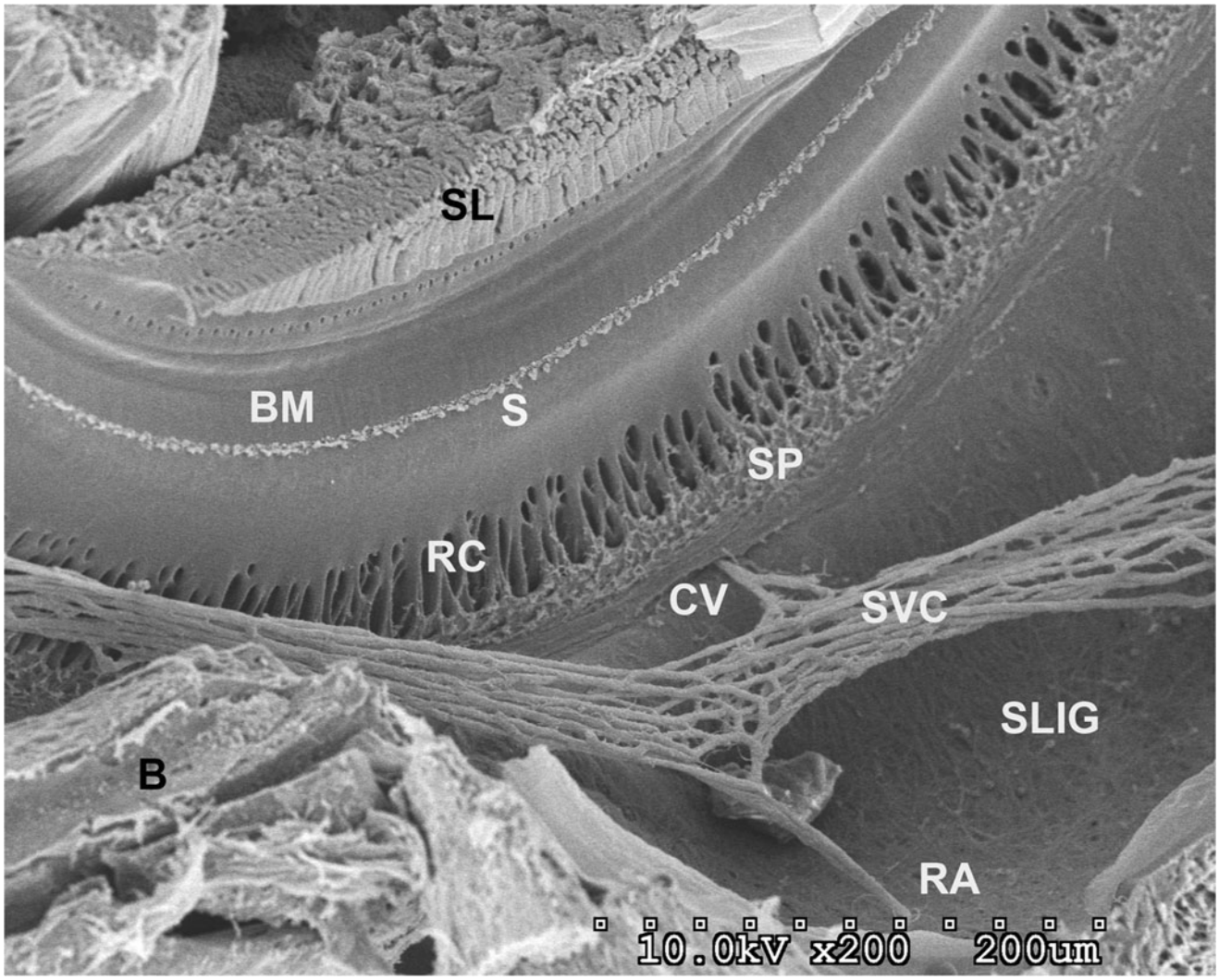

FIG. 2. Lower magnification SEM view of the basal end of the scala media showing the bone (*B*), spiral limbus (*SL*), basilar membrane (*BM*), upon which resides the newly described structure (*S*), the openings of the root cell processes (*RC*), the spiral prominence (*SP*), basement membranes of the capillaries of the stria vascularis (*SVC*), collecting venule (*CV*), radiating arteriole (*RA*), and the spiral ligament (*SLIG*).

disappearance of Boettcher cells in the cochlear apex. Lateral to the structure is more smooth membrane surface and then up the lateral wall there appear numerous oval-shaped openings of variable diameters in the lateral wall.

Fibrillar material lines the apical portion of the openings and extends into the spiral prominence. More lateral is a small (~15 μm) spirally directed band of ECM that lies adjacent to a broad area of spiral ligament that was previously in contact with the border cells of the stria vascularis. A free-floating network of stria vascularis capillary basal lamina is also present. This network of tubules is attached to the lateral wall by the collecting venules and the radiating arterioles (Fig. 2).

We will describe the ECMA dark spirally directed line of different structures in more detail from the medial to the lateral wall of the scala media. The spiral limbus appears as a collection of columnar plates with the teeth of Huschke at the front edge (Fig. 3a, b). Each plate is surrounded by a smooth basal lamina. Beneath the spiral limbus is another smooth membrane lining the internal sulcus region that is perforated by the habenula perforata (Fig. 3a, c). There are approximately 25 habenula perforata per 100 μm of basilar membrane length, and the openings are divided into two size categories: 0.25 μm and 2 μm with the larger openings dominating their distribution. Figure 3b shows the spiral limbus at the basal end of the scala media. The limbus fragments into small heads of the columnar plates and the whole area appear to be covered by basal lamina. A small portion of the basal lamina of Reissner's membrane is also present in this Fig. Figure 3c is a fractured surface through the osseous spiral lamina showing a channel from the habenula

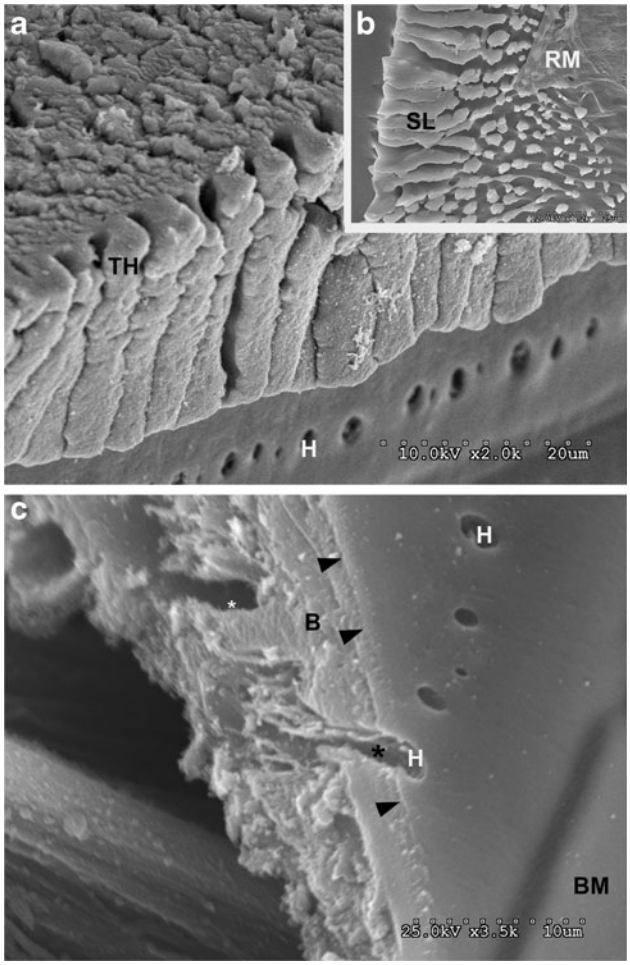

FIG. 3. **a** SEM view of the spiral limbus in a decellularized cochlea showing basal lamina coated columns of ECM, the teeth of Huschke (*TH*) and the habenula perforata (H) with a diameter of approximately 2 μm. **b** The spiral limbus (*SL*) at the basal end of the cochlea where there is extensive basal lamina covering heads of the smaller pillars. A small portion of the basal lamina of Reissner's membrane (*RM*) is also present. **c** A fracture through the osseous spiral lamina and a habenula perforata (*H*) showing the extension of the channels where the nerves travel through the habenula (*). The basilar membrane is shown on the lower right (*BM*), and the *arrowheads* indicate the coating of basal lamina material over the bone (*B*).

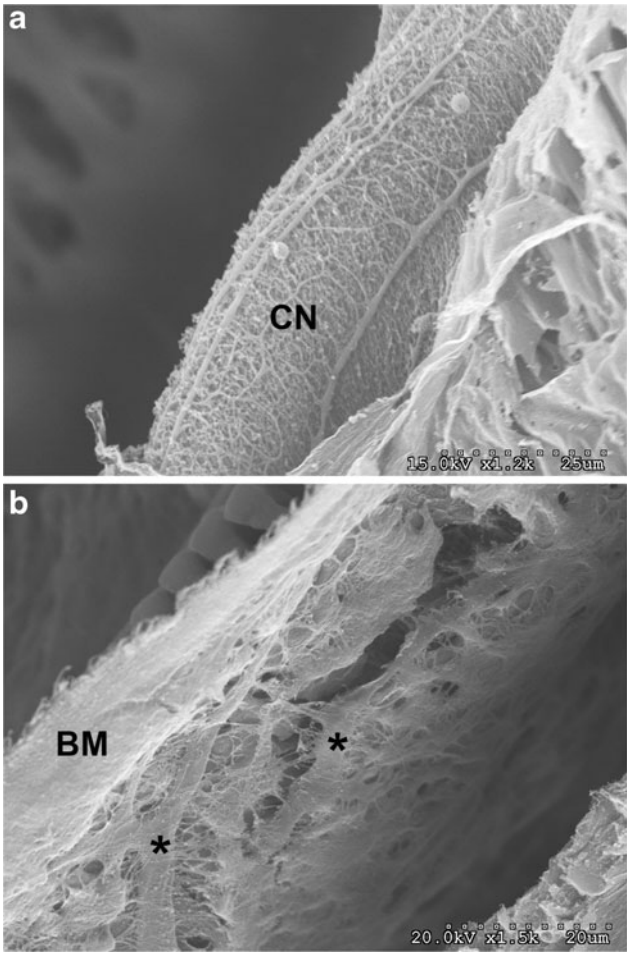

FIG. 4. **a** The apical surface of a small portion of the tectorial membrane is present and shows the cover net (CN) and underlying collagenous matrix of the membrane. **b** A cross section and a portion of the undersurface of the basilar membrane (BM). Deeper layers are the undersurface of the osseous spiral lamina that lies within the scala tympani. The bony layers show openings, fibrils and strands of material in this matrix (*).

perforata. One can also see a thin layer (arrowheads) above the osseous spiral lamina that appears to be the basal lamina lining the surface of the inner hair region.

With the dissolution of the interdental cells of the tectorial membrane and the stereocilia of the outer hair cells, both attachments of the tectorial membrane were removed, and it was usually washed out of the cochlea during perfusion of the decellularization solution. However, we were able to obtain a few images of the tectorial membrane after decellularization. Figure 4a shows the apical surface of the tectorial membrane that shows strands of the cover net and the underlying fibrillar matrix of the tectorial membrane. In addition, another structure that was difficult to image in SEM was the undersurface of the basilar membrane. Figure 4b shows a cross-section of the basilar membrane and its undersurface. The cross-section shows homogenous and fibrillar material, and the undersurface of the osseous spiral lamina shows thick strands of material and fine filaments.

Figure 5 is an SEM from a cochlea that was processed by the OTO method, which increases electron density by precipitation of osmium tetroxide by thiocarbohydrizide onto the specimen. This method made the structure more apparent but it produced globular artifacts. A dark spirally directed line (arrow) marks the beginning of the underlying basilar membrane. This smooth layer of basal lamina extends over the basilar membrane to a lighter area and then to a darker, marked depression in Figure 5a. Based upon a distance measurement of 16 μm, this depression appears to correspond to that region of the basilar membrane which was covered by inner and outer

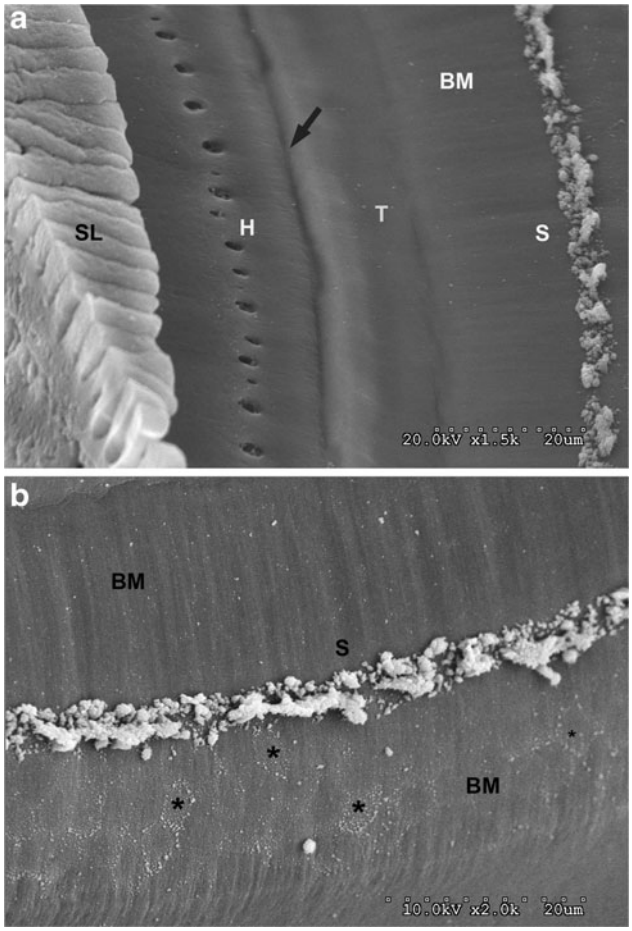

FIG. 5. **a** SEM of a decelluarized cochlea showing the spiral limbus (*SL*), habenula perforata (*H*), and the medial beginning of the basilar membrane as indicated by a spirally directed dark line (*arrow*). Light and darker areas are more lateral (*T*) where presumably the tunnel cells use to lie, and then, the smooth surface basilar membrane extends to the structure (*S*) shown in an OTO processed cochlea. **b** A higher magnification view of the basilar membrane (*BM*), structure (*S*), and numerous pentagonal/hexagonal imprints of the Boettcher cells (*) on the side of the structure facing the lateral wall.

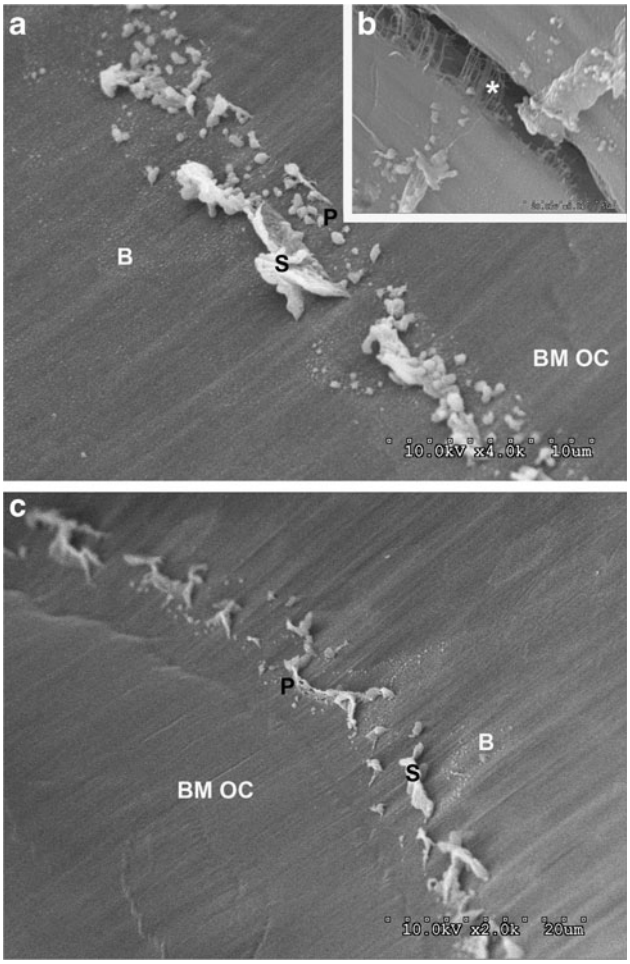

FIG. 6. **a** SEM views of the structure from a decellularized cochlea not processed with OTO. It forms a spirally directed, single line of periodic structures. They show septa-like (*S*) protrusions from the basilar membrane on the Boettcher side (*B*) of the basilar membrane and particles (*P*) on their side facing the organ of Corti (*BM OC*). **b** Higher magnification insert shows a crack in the basilar membrane and fine filaments extending radially in the deeper layers of the basilar membrane. **c** Another cochlea showing similar morphology of the structure with a periodic distribution, septa, particles, and imprints. Radial and some spiral striations appear in the basilar membrane.

tunnel cells of the organ of Corti. More lateral is a wider area (24 μm) over which the hair cells and supporting cells of the organ of Corti presumably resided, until one encounters the spirally directed structure at the border of Hensen's and Boettcher cells. Figure 5b is a higher magnification of the structure on the basilar membrane, and one can see apparent cell imprints on the lateral side of the structure. These imprints likely mark the base and borders of Boettcher cells, thus further locating the structure along the radial width of the basilar membrane. Although the basilar membrane is relatively smooth it also exhibits radial striations throughout its width (Figs. 5 and 6).

However, most of our specimens were not processed by the OTO method, and the morphology of the structure appears to be more likely composed of septa (5 μm tall) with particles (0.5 μm in diameter) (Fig. 6a, b, c). The septa face Boettcher cells and the particles face the organ of Corti (Fig. 6a, b). The structure seems to have a periodic distribution (6-μm spacing) as it extends spirally. In addition to prominent radial striations along the surface of the basilar membrane, spirally directed striations are also present (Fig. 6a, b). Cracks in the basilar membrane due to processing artifact show thin filaments extending in a radial direction in deeper layers of the basilar membrane (Fig. 6b). The basilar membrane extended for approximately 43 μm laterally until there was another dark depression that marked the end of the basilar membrane (Fig. 1b).

At the basilar crest end of the basilar membrane, a smooth region of ECM extended apico-laterally until one encountered a series of small (4 × 6 μm) and large (5 × 30 μm) oval-shaped openings in the ECM (Fig. 7a, b). At the apical end of the cochlea, these holes were more circular and less numerous. The basal surface of these openings was smooth like the rest of the basilar membrane and is lined with basal lamina. The apical surface of the large openings has overlying filamentous ECM material (0.5 μm in diameter) and extends into the elevated ridge of the spiral prominence (Fig. 7a, b). Within the ridge of the spiral prominence, the ECM also forms septa-like oval or circular patterns (5 μm in diameter) (Fig. 7b). Above the spiral prominence is a striated band of spirally directed ECM that is 15-μm wide (Figs. 7b and 8).

Figure 8a shows the network of capillary basal lamina of the stria vascularis. The capillary basal lamina appears as a branched network of tubules with a diameter of 3 μm, which are associated with some very thin (0.3 μm) filaments (Fig. 8a). Figure 8b shows abroad region of loose mesh-like arrangement of fibrous ECM of the spiral ligament that faced the basal cell layer of the stria vascularis adjacent to this band. These fibers are approximately 5 μm in diameter and form an interconnecting mesh of fibers that travel orthogonal

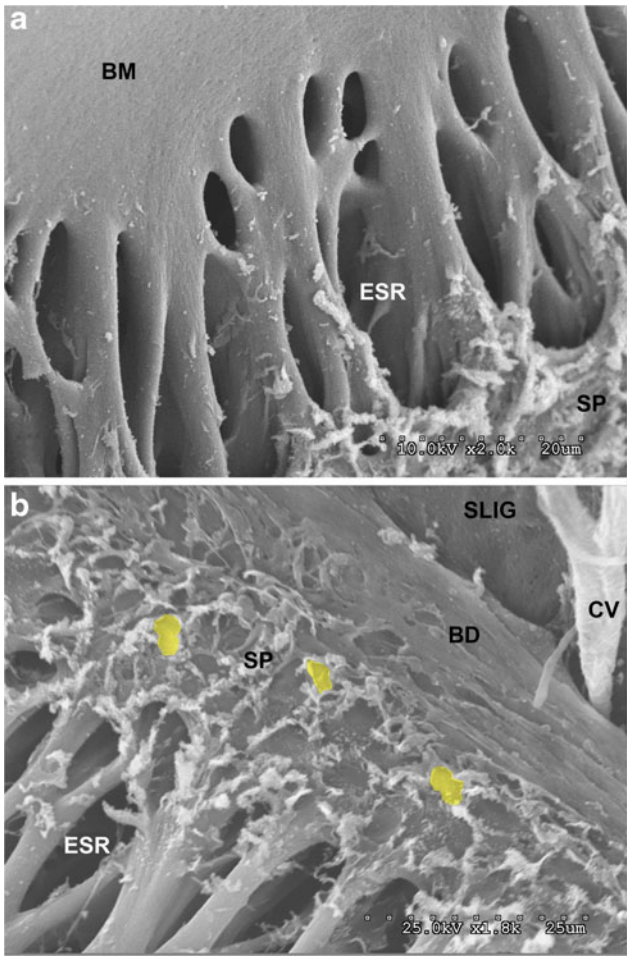

FIG. 7. **a** In a continuous extension up the lateral wall is the smooth surface material (i.e., basal lamina) that coats small and large openings that previously contained the root processes of the outer sulcus (*ESR*). At the apical end of these openings, filamentous material is present and extends into the spiral prominence (*SP*). **b** The spiral prominence (*SP*) region exhibits short, septa-like extensions that appear to have previously surrounded the spiral prominence epithelial cells (*yellow-filled areas*). Further up the lateral wall is a spirally directed band of filaments (*BD*) that is approximately 15 μm in width. A collecting venules (CV) is also seen penetrating the lateral edge of this bundle and the underlying spiral ligament (SLIG).

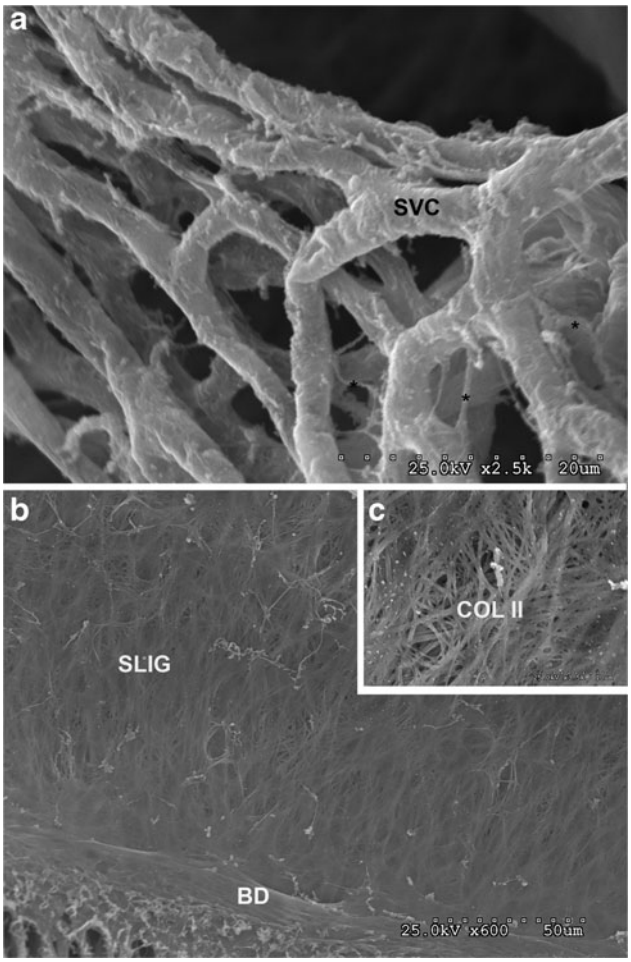

FIG. 8. **a** A network consisting of the basal lamina of the capillaries of the stria vascularis (*SVC*). The capillaries are approximately 3 μm in diameter, branched and are associated with a fine network of thin (0.3 μm) filaments (*). The capillary basal lamina appears to be "free floating" above the spiral ligament and are connected to the lateral wall by the collecting venues and radiating arterioles. **b** The spiral ligament (SLIG) is composed of a meshwork of filaments that are 5 μm in diameter or smaller. The surface facing the previous stria vascularis is relatively smooth and consists of a loose network of cross-connecting filaments. A band (*BD*) lies between the spiral prominence and the spiral ligament. **c** Insert shows details of these filaments which are presumably collagen II (COL II).

and longitudinal to one another (Fig. 8c). These fibers are presumably composed of type II collagen. A cross-section through spiral ligament (Fig. 9a, b) showed numerous openings (5–7 μm in diameter) that lie within the meshwork of fibers and presumably housed the fibrocytes. Rosenthal's canal also showed numerous openings (15 × 3 μm in diameter) (Fig. 10a, b). Perineurial basement membrane material lined these openings as well as additional ECM material. In deoxycholate decellularized cochleas, undissolved cellular residue was also observed in the larger openings in Rosenthal's canal (Fig. 10b). This material was not observed following SDS detergent extraction. Figure 10c is a higher magnification view of one of the openings that presumably housed the spiral ganglion neurons. It is surrounded by fenestrated basal lamina, which forms a looser network of material than was observed along the basilar membrane surface. Additional fibrillar ECM also appears to surround the openings (Fig. 10c).

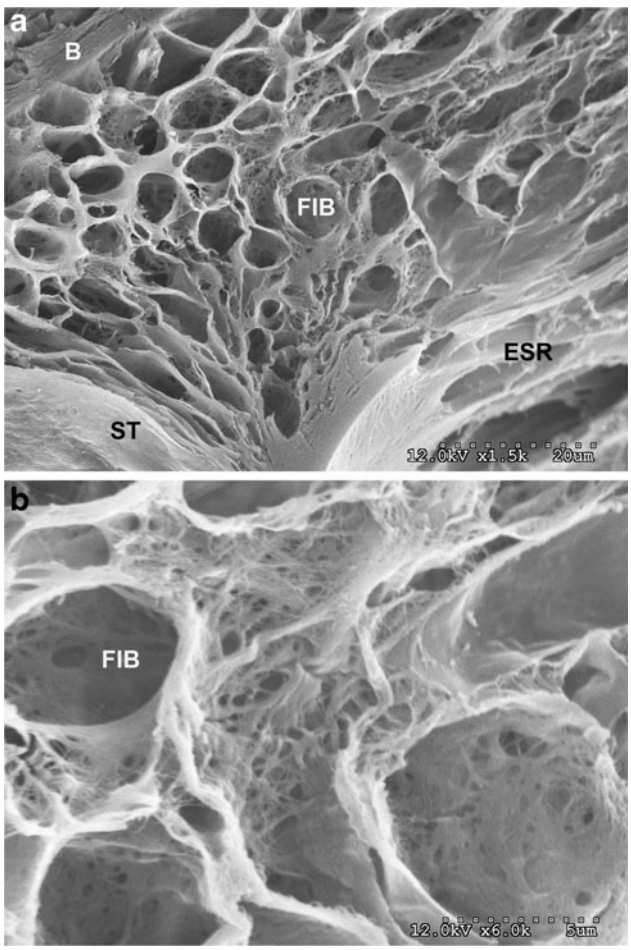

FIG. 9. This figure shows surface of the scala tympani (ST) on the left, a cross-section of the spiral ligament at the top with openings, which previously contained fibrocytes (*FIB*) and a portion of the scala media with the external sulcus cell openings. **b** Shows the filamentous network of the spiral ligament and the openings (*FIB*) previously occupied by fibrocytes that are surrounded by type II collagen filaments.

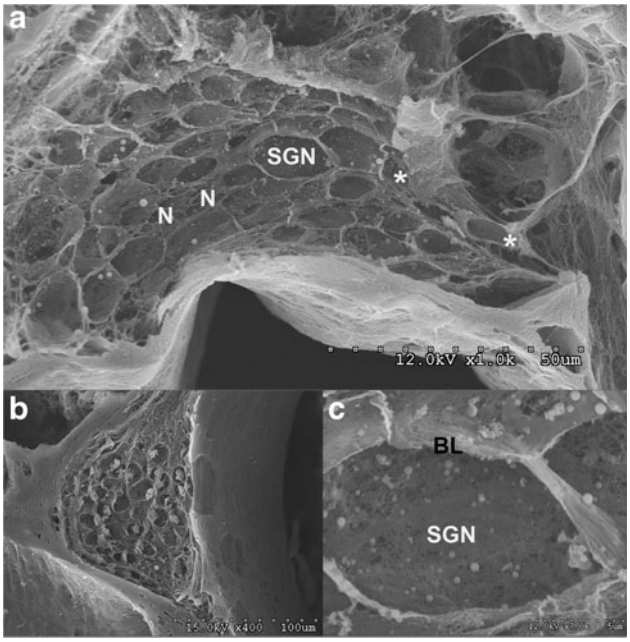

FIG. 10. **a–c** SEM views of Rosenthal's canal and the spiral ganglion. **a** Numerous empty openings that previously housed the spiral ganglion neurons (*SGN*) are evident (15 μm in diameter) as well as openings for nerve fibers (*N*) (3 μm in diameter) and where the cell bodies extended into the nerve processes (*). **b** In a deoxycholate-treated cochleas, the contents of the spiral ganglion neurons were not completely extracted by the detergent therefore a residue remains. **c** Higher magnification view of an opening that previously contained a spiral ganglion neuron (*SGN*) surrounded by basal lamina material (*BL*) and additional fibrillar ECM material.

Human Cochlea

sTSLIM and SEM views of the decellularized human cochlea confirmed our previous observations on decellularized mouse and rat cochleas (Santi and Johnson 2013), namely that a significant portion of the membranous labyrinth is composed of ECM. Figure 11 shows a direct volume rendering cross section of the basal turn of the scala media after sTSLIM imaging (a) and then after SEM imaging (b). The volume rendering after sTSLIM imaging resembles the SEM view of the same specimen. Prominent cochlear ECM structures are present, including the following: the bone, spiral limbus, basilar membrane, spiral prominence, spiral ligament, and basal lamina of the stria vascularis capillaries. Further observations on prominent ECM structures will be described from the medial to lateral edge of the scala media.

The spiral limbus appears as columnar plates of ECM separated by openings on the apex of the spiral limbus (Fig. 12a). The habenula perforata are seen as a spirally-directed, single line of openings beneath the spiral

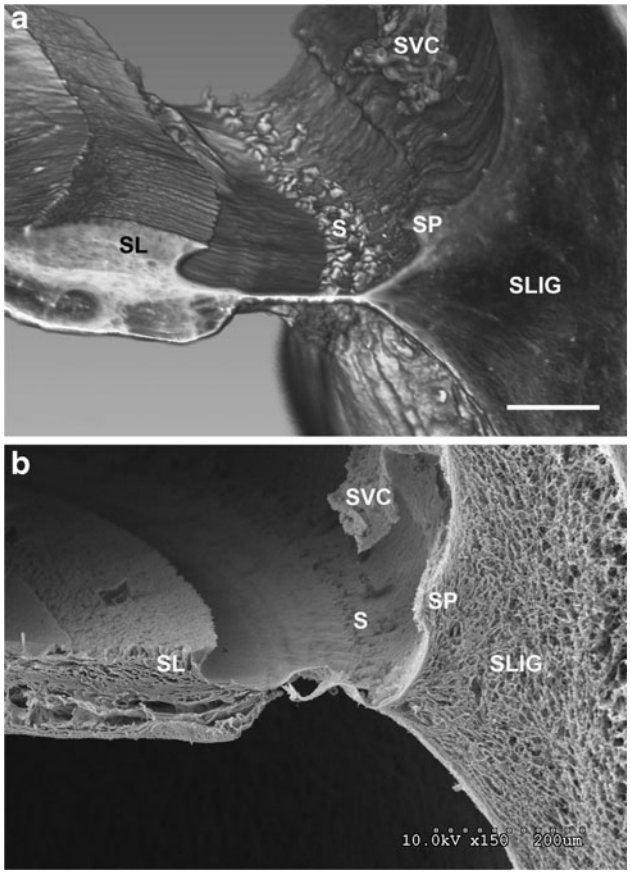

FIG. 11. **a** A direct volume rendering of 150, 8 μm sTSLIM cross section of the scala media in a decellularized human cochlea from a basal turn. Note the spiral limbus (*SL*) and multiple structures (*S*) on the basilar membrane. The spiral prominence (*SP*), the basal lamina of the stria vascularis capillaries (*SVC*), and the spiral ligament (*SLIG*) are also present. *Bar* = 100 μm. **b** An SEM view of the same specimen as in panel a showing the spiral limbus (*SL*) structure (*S*) on the basilar membrane, spiral prominence (*SP*), basal lamina of the stria vascularis capillaries (*SVC*), and the spiral ligament (*SLIG*).

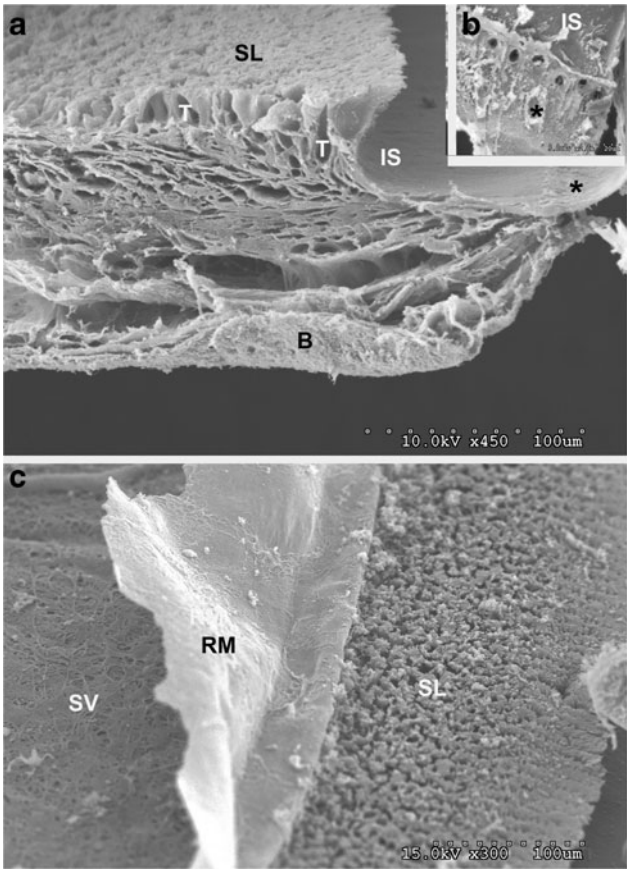

Fig. 12. **a** Higher magnification SEM view of the basal end of the scala media showing the bone (*B*), spiral limbus (*SL*) with spaces where the interdental T cells occupied (*T*), inner sulcus (*IS*), and inner hair cell region near the habenula perforata (*). **b** View of inner sulcus cell region (*IS*), the openings of the habenula perforate and septa-like features (*) at the basal border of the cells at the inner hair cell region. **c** Lower magnification view of the bone of the scala vestibule (*SV*) showing fibers and openings, the basal lamina of Reissners membrane (*RM*), and the apical portion of the spiral limbus (*SL*) showing openings between the heads of the spiral limbus plates.

limbus (Fig. 12b. Lateral to the habenula perforata are septa-like features that appear to be basal outlines of cells in the region of the inner hair cells. A top-down view of the spiral limbus shows distinct radial rows of ECM that are the teeth of Huschke (Fig. 12c). Toward the attachment of Reisssner's membrane, these rows turn into discrete heads of ECM that are surrounded by openings in the top of the limbus. Portions of Reissner's membrane are still attached at the medial edge of the spiral limbus, and it appears similar to the apical surface of the basilar membrane with a smooth morphology. More medial to the attachment of Reissner's membrane is the surface of the bone of the scala vestibule (Fig. 12c). The bone exhibits numerous crossing fibrils interspersed with openings into the underlying bone.

Lateral to the habenula perforata, the basilar membrane is relatively smooth with the exception of scattered globular material until one encounters a spirally directed series of septa-like structures that form two or more rows (Figs. 11 and 13). The septa are approximately ~25 μm in height and ~10 μm in width. They are discrete, periodic structures that travel in radial and spiral directions along the basilar membrane. In human, they form several rows (Figs. 11 and 13a). Above the basilar membrane appears a "free-floating" network of tubules that is the basal lamina of the stria vascularis capillaries (Figs. 11 and 13b). The tubules have open lumens, and each tubule is surrounded by a thick (~3 μm) basal lamina that extends and intermingles with other tubules laterally to form a network of tubules (Fig. 13b).

The spiral prominence is a spirally directed ridge of tissue that extends into the scala media (Fig. 14). Along its apical surface are numerous septa-like features that appear to be outlines of cells of the former spiral prominence epithelial cells (Fig. 14a). Along the basomedial surface of the spiral prominence and above the basilar crest is a single row of spirally directed openings

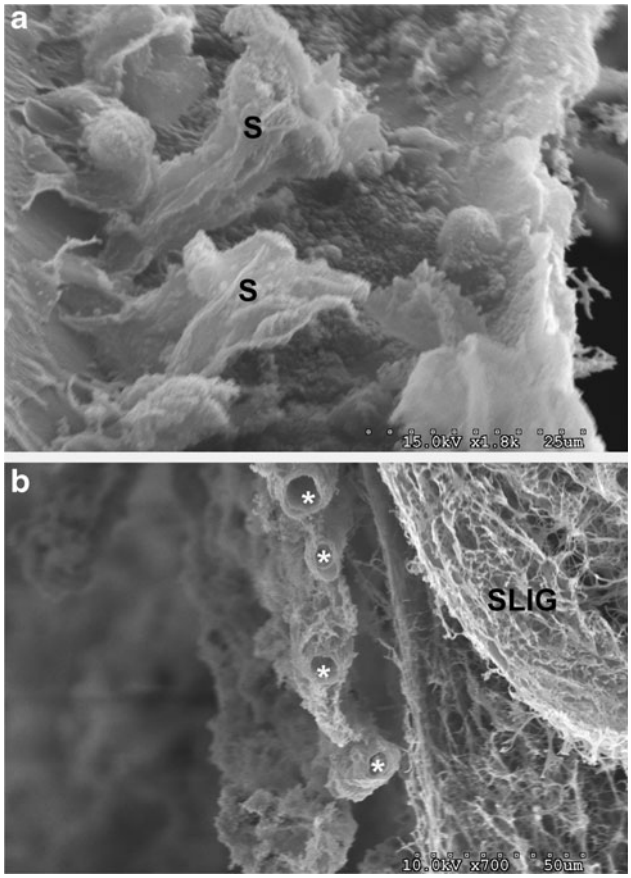

FIG. 13. **a** SEM view of the spirally directed structures on the apical surface of the basilar membrane showing long septa-like features (*S*). **b** Adjacent to the spiral ligament (*SLIG*) are "free-floating" basal lamina of the stria vascularis capillaries showing thick basal lamina and hollow lumen (*).

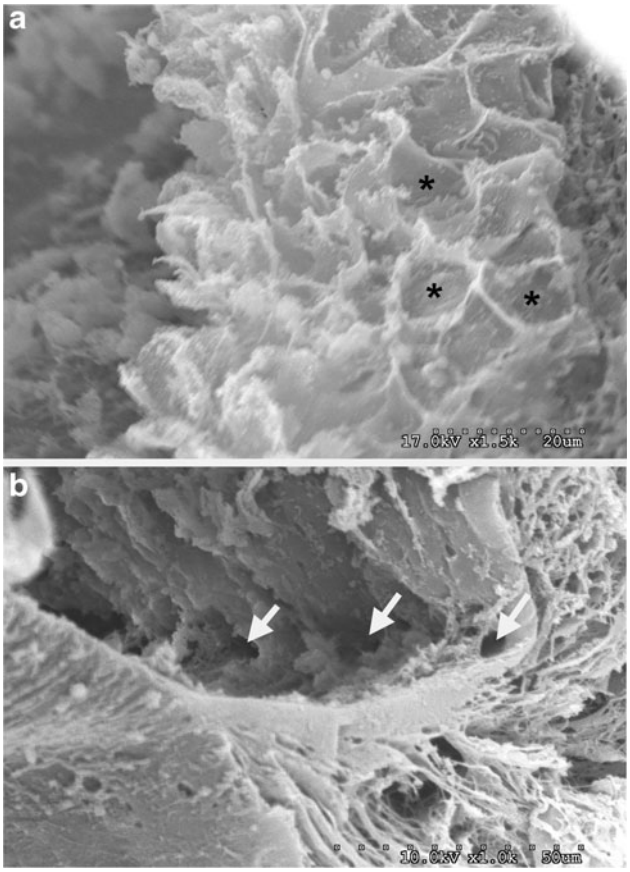

FIG. 14. **a** The spiral prominence is a raised ridge of ECM near the basilar crest of the lateral wall that shows septa-like structures that appear to outline the previous basal borders of the spiral prominence epithelial cells (*). **b** The lower border of the spiral prominence showing a single row of openings (~5 μm in diameter) into the adjacent spiral ligament ECM that presumably housed the root cells (*arrows*).

that are approximately 7 μm in diameter (Fig. 14b). These openings, which presumably housed the root cells, extend into channels that travel into the underlying spiral ligament. A cross-section through the lateral wall of scala media shows a large ECM structure of the spiral ligament (Fig. 15a). On its lateral surface is the bony structure of the otic capsule and within its matrix are numerous filaments surrounding fusiform openings. Toward the bone, the spaces between the filaments appear larger. Adjacent to the spiral ligament is the scala media with its floor formed by the basilar membrane showing the structures along its spiral length (Fig. 15a). Figure 15b shows the scala tympani surface of the basilar membrane where it joins with the bony surface of the osseous spiral lamina. The osseous spiral lamina exhibits rows of radially directed bony structures covered by filaments and globules. The undersurface of the basilar membrane shows a globular matrix. Rosenthal's canal is medial to the spiral limbus and near the modiolus (Fig. 16). It is a spirally directed channel with fibers, spherically shaped openings (~60 μm in diameter) and smaller openings. Figure 16b shows a higher magnification of one of these openings, which is lined by an open network of filaments and presumably housed the spiral ganglion cell neurons.

DISCUSSION

SEM observations of the decellularized cochlea showed that a major portion of the membranous labyrinth is extracellular matrix and not cellular. The bone is present as well as other recognizable structures, including the following: spiral limbus, Reissner's membrane, basilar membrane, spiral prominence, external sulcus root cell openings, spiral ligament, the capillary basal lamina of the stria vascularis, and the ECM of Rosenthal's canal. The most prominent missing features are cells of the organ of Corti and their neural innervation. Cells of the stria vascularis are missing as well as other epithelial and connective tissue cells of the scala media.

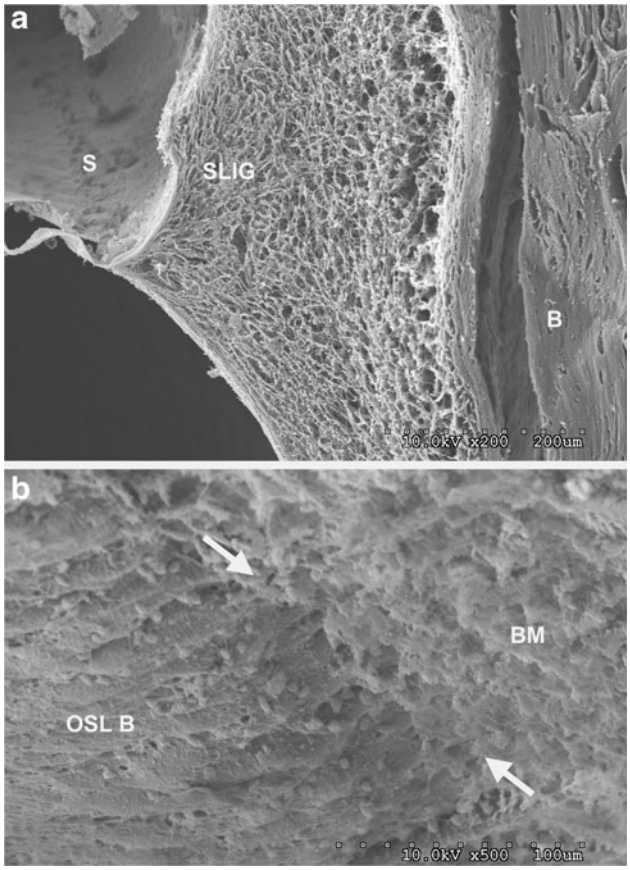

FIG. 15. **a** A cross-section of the scala media showing the otic capsule bone (*B*), a fibrous network of filaments and fusiform-shaped openings in the matrix of spiral ligament (*SLIG*), and the structures (*S*) along the lateral edge of the basilar membrane. **b** The undersurface of the medial edge of the bone of the osseous spiral lamina (*OSL B*) where it meets (*arrows*) the basilar membrane (BM). The bone shows radial ridges of ECM whereas the basilar membrane contains filaments and globular materials.

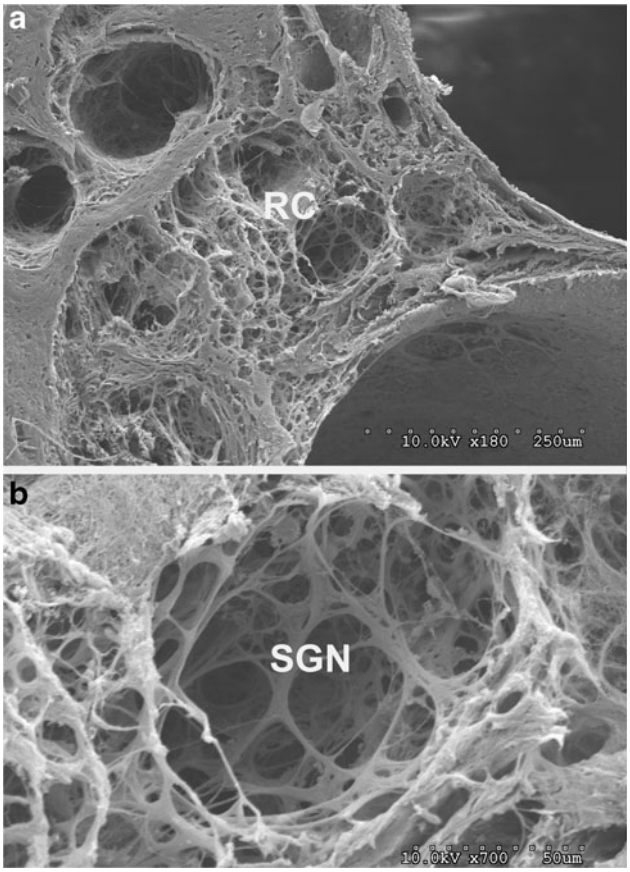

FIG. 16. **a** A cross-section of Rosenthal's canal showing fibrous elements and openings. **b** A spherical-shaped opening (SGN) which presumably housed the spiral ganglion neurons surrounded by loose ECM filaments.

Decellularization of the cochlea revealed new observations on the ECM especially in regard to viewing ECM components in 3D rather than in 2D sections of tissues. In a previous study at the light microscope level, sTSLIM observations revealed a new, spirally directed structure along the basilar membrane. SEM views of this structure verify its position at the border of Hensen/Boettcher cells and further details of its morphology. It consists of septa-like structures on its lateral side and particles on its modiolar side. Due to its periodic structure, it seems to be cell associated but extracellular. We (Liu et al. 2015) showed that the structure was reactive to antibodies to type IV collagen and laminin, further supporting its ECM composition. It appears that the septa line Boettcher cells and the particles are associated with the Hensen cells, at least in the mouse. The structure appears as a single row in the mouse (Figs. 1b and 2, 5, 6) and multiple rows with more extensive septa in the human (Figs. 11 and 13a). The function of this structure is unknown but it disappears apically similar to the distribution of Boettcher cells. Mammano and Ashmore (1993) and Nobili et al. 1998 describe the hydrodynamic interactions within the organ of Corti that give rise to frequency selectivity by suppression of adjacent frequencies. Anatomically, the organ of Corti distorts under outer hair cell contraction and pivoting occurs around the inner attachment of the basilar membrane. This would require a strong attachment of the organ of Corti at the lateral aspect of basilar membrane at the Hensen cells, and perhaps this is accomplished by the newly described septa-like ECM structures surrounding the base of Hensen cells?

Another notable feature of decellularized cochleas is uniform distribution of the basal lamina as viewed as a 3D sheet of smooth material vs. as a thin line that appears in cross sections. However, the surface of the basilar membrane in the organ of Corti region in the human showed more globular material than in the mouse. This was consistent across all human and mouse specimens, and it might be due to the older age of the humans compared with the younger age of the mice? Santi and Johnson (2013) reported the presence of type IV collagen and laminin in

decellularized tissues, and this smooth surface likely contains these ECM components. Tsuprun and Santi (1999) also reported the presence of other basal lamina components such as nidogen/entactin and perlecan but it is not known whether these components survive the decellularization process. Fractures in the basilar membrane showed radial fibers that are presumably type II collagen embedded in the matrix of fibronectin and tenascin within the basilar membrane that have been previously reported (Santi et al. 1989; Swartz and Santi 1999).

At the basal end of the cochlea, the spiral limbus consists of small heads of the plates and teeth of Huschke. However, the spiral limbus grows in width and thickness toward the cochlear apex. Basal lamina covers the apical portion of the spiral limbus columns as it lines the basal portion of the interdental cells. In the mouse, the teeth of Huschke appear more distinct, blunt columns (Figs. 2, 3, and 5) compared with the human (Fig. 12), but they appear mostly similar. The habenula perforata lie beneath the inner sulcus, and the basal lamina continues over these structures. The channels of the habenula perforata are hollow as all the cytoplasmic components of the nerve fibers have been removed. In the mouse (Figs.3 and 5a), these openings and channels vary in size but are mostly a large diameter, presumably to accommodate greater numbers of nerve fibers. In the human, the habenula are more uniform in size (Fig. 12b).

As mentioned previously, with the attachments of the tectorial membrane, namely, the interdental cells and the outer hair cell stereocilia, dissolved by detergent the tectorial membrane is usually lost from the cochlea during solution perfusion. However, a small portion of it was observed in SEM. The tectorial membrane is acellular and composed of ECM therefore one would not expect it to be dissolved by the detergent. In fact, we observed it in the mouse cochlea to exhibit the apical cover net and underlying collagenous filaments that have been previously described (Tsuprun and Santi 2001).

Basal extracellular imprints on the basilar membrane were present for Boettcher cells in the mouse (Figs. 5b and 6), cells in the inner hair cell region of the human (Fig. 12b), but not other cells such as the supporting cells, pillars, Deiters and Claudius cells. However, imprints and surrounding septa were observed for spiral prominence epithelial cells in both the mouse (Fig. 7b) and human (Fig. 14a). Previous TEM observations of Boettcher cells do show numerous invaginations along their basal surfaces (Santi 1988; Kanazawa et al. 2004) which could be occupied by ECM that we see in decellularized cochleas. The beginning and end of the basilar membrane is marked by a dark line and depressions in SEM. In addition, a change in density and a depression of the basilar membrane appears to coincide with the pillar cell region of the organ of Corti.

In the lateral wall above the basilar crest, there are numerous oval-shaped openings that are lined with basal lamina material in the mouse only (Figs. 1b, 2, and 7). In the human, these openings are reduced to a single row of uniform size (Fig. 14b). These openings have been previously occupied by the root cells of the outer sulcus. Jagger and Forge (2013) recently provided a detailed review of these cells. They conclude that root cells regulate the solute content of the endolymph and/or perilymph and may be essential in the homeostasis of the cochlea. Fluid-transporting enzymes, gap junctions, and K^+ recycling properties of these cells were also reviewed. However, the striking difference in morphology between these cells in the mouse and the human reported in this communication has not been related to a functional difference between the two species. Since these openings are greatly reduced in humans, it probably means that the human has fewer numbers and/or volume of root cells. We also observed a new description of fibrils, in the mouse cochlea, at the apical portion of these openings, which extends into the spiral prominence. New septa-like projections are numerous along the spiral prominence and presumably surrounded the spiral prominence epithelial cells.

Adjacent to the spiral prominence is another new structure consisting of a spirally directed band of filaments in the mouse cochlea. These filaments appear to run along the edge of the border cells of the stria vascularis that is adjacent to the spiral prominence. The surface of the spiral ligament that faces the basal cells of the stria vascularis is flattened and consists of a meshwork of filaments that are presumably composed of collagen type II. No basal lamina is present in this area, and we do not see the smooth sheet of material that was present on the apical surface of the basilar membrane. Cross-sections of the spiral ligament showed openings that presumably contained the fibrocytes that are embedded in a meshwork of collagen II fibers. These openings appear spherically shaped in cross-sections.

With the dissolution of the cells of the stria vascularis, the only component remaining is the basal lamina of its capillaries. The network appears to be “free floating” within the scala media but it is attached to the lateral wall by the collecting venues and the radiating arterioles. Newly described thin fibrils are associated with this capillary basal lamina in the mouse cochlea. The basal lamina of the capillaries of the stria vascularis is of interest for functional reasons since it appears similar to the kidney glomerular basal lamina in that it is wide and may be the result of fusion of epithelial and endothelia basal lamina. It has been involved in novel peptides of type IV collagen that are related to Alport syndrome (Kleppel et al. 1989a, b) and have been shown to increase in width in a murine animal model of Alport syndrome (Cosgrove et al. 1998). Decellularized stria vascularis basal lamina

may be a useful way to investigate the unique properties of these capillaries. Stria vascularis capillary basal lamina was much thicker in the human than in the mouse and may be due to aging in the humans.

Examination of Rosenthal's canal revealed hollow openings and tubes that were previously occupied by spiral ganglion neurons and their processes. In deoxycholate decellularized cochleas, cell debris remains in the openings left by the spiral ganglion neurons, and we interpret this as an extraction and diffusion artifact from the weaker detergent compared with SDS. This was also observed in sTSLIM sections (Santi and Johnson 2013). Although it is well known that the cell bodies and nerve processes are surrounded by basal lamina, it did not appear like the basal lamina in other areas of the cochlea, such as along the basilar membrane. It appeared fenestrated, and an underlying collagenous matrix was also observed. It is not known why it does not appear as a continuous sheet similar to other cochlear basal lamina.

Decellularized cochlea examined by SEM has provided interesting new observations on the ECM of the cochlea. Differences were noted in the ECM of the mouse and human that may turn out to have functional significance. The most noteworthy feature in decellularized cochleas was the spirally directed structure along the basilar membrane. SEM has also revealed new observations of the cochlear ECM that we did not resolve in sTSLIM serial sections, including the following: fibers at the apex of the root cell process openings in the mouse, septa-like borders around the spiral prominence epithelial cells, fine filaments associated with the basal lamina of the stria vascularis capillaries in the mouse, and a band of filaments between the spiral prominence and the stria vascularis in the mouse. Decellularization may also be a new useful tool to isolate cochlear structures for further investigations, such as the tectorial membrane and basal lamina of the stria vascularis capillaries. Lastly, it will be interesting to determine if the cochlear ECM has inductive cues that stem cells can use to differentiate into different cochlear tissues such as neurons, hair cells, supporting cells, epithelial cells, and connective tissue cells such as fibrocytes.

ACKNOWLEDGMENTS

The authors would like to thank Meredith Adams, M.D., for perfusing one of the human cochleas with SDS. Funding was provided to PAS by the NIDCD (RO1DC007588, U24DC011968), the Capita Foundation, and the Lions Hearing Foundation. The authors would like to thank Gail Celio at the University Imaging Centers for excellent assistance with SEM. Additional funding was supported by research of the European Community Research, Human stem cell applications for the treatment of hearing loss. Grant agreement no. 603029. Project acronym: OTOSTEM (HRA).

REFERENCES

Cosgrove D, Samuelson G, Meehan DT, Miller C, McGee J, Walsh EJ, Siegel M (1998) Ultrastructural, physiological, and molecular defects in the inner ear of a gene-knockout mouse model for autosomal Alport syndrome. Hear Res 121:84–98

Duvall A, Flock A, Wersall J (1966) The ultrastructure of the sensory hairs and associate organelles of the cochlear inner hair cells, with reference to directional sensitivity. J Cell Bio 24:497–505

Engstrom H (1951) Microscopic anatomy of the inner ear. Acta Otolaryng 40:522

Friedmann I (1962) The cytology of the ear. Brit Med Bull 18:209–213

Iurato S (1967) Submicroscopic structure of the inner ear. Pergamon Press, London

Jagger DJ, Forge A (2013) The enigmatic root cell—emerging roles contributing to fluid homeostasis within the cochlear outer sulcus. Hear Res 303:1–11

Kanazawa A, Sunami K, Takayama M, Nishiura H, Tokuhara Y, Sakamoto H, Iguchi H, Yamane H (2004) Probable function of Boettcher cells based on results of morphological study: localization of nitric oxide synthase. Acta Otolaryngol Suppl 554:12–6

Kleppel MM, Santi PA, Cameron JD, Wieslander J, Michael AF (1989a) Human tissue distribution of novel basement membrane collagen. Am J Pathol 134:813–825

Kleppel MM, Kashtan C, Santi PA, Wieslander J, Michael AF (1989b) Distribution of familial nephritis antigen in normal tissue and renal basement membranes of patients with homozygous and heterozygous Alport familial nephritis. Relationship of familial nephritis and Goodpasture antigens to novel collagen chains and type IV collagen. Lab Invest 61:278–289

Lim DJ (1969) Three dimensional observation of the inner ear with the scanning electron microscope. Acta Otolaryng Suppl 255

Lim DJ (1970) Morphology and function of the interdental cell an ultrastructural observation. J Laryngology Otology 84:1241–1256

Liu W, Atturo F, Aldaya R, Santi P, Cureoglu S, Obwegeser S, Glueckert R, Pfaller K, Schrott-Fischer A, Rask-Andersen H (2015) Macromolecular organization and fine structure of the human basilar membrane—RELEVANCE for cochlear implantation. Cell Tissue Res 360:245–262

Mammano F, Ashmore JF (1993) Reverse transduction measured in the isolated cochlea by laser Michelson interferometry. Nature 365:838–841

Nobili R, Mammano F, Ashmore J (1998) How well do we understand the cochlea? TINS 21:159–166

Santi PA (1988) Cochlear microanatomy and ultrastructure. In: Physiology of the Ear, Eds., AF Jahn and FR Santos-Sacchi. Raven, New York, pp 173–199

Santi PA, Johnson SB (2013) Decellularized ear tissues as scaffolds for stem cell differentiation. JARO 14:3–15

Santi PA, Larson JT, Furcht LT, Economou TS (1989) Immunohistochemical localization of fibronectin in the chinchilla cochlea. Hear Res 39:91–101

Seligman AM, Wasserkrug HL, Hanker JS (1966) A new staining method (OTO) for enhancing contrast of lipid-containing membranes and droplets in osmium tetroxide-fixed tissue with osmiophilic thiocarbohydrazide (TCH). J Cell Biol 30:424–432

Smith CA, Sjoestrand FS (1961) Structure of the nerve endings on the external hair cells of the guinea pig cochlea as studied by serial section. J Ultrastruc Res 5:523–556

Swartz DJ, Santi PA (1999) Immunolocalization of tenascin in the chinchilla inner ear. Hear Res 130:108–14

Tsuprun V, Santi PA (1999) Ultrastructure and immunohistochemical identification of the extracellular matrix of the chinchilla cochlea. Hear Res 129:35–49

Tsuprun V, Santi PA (2001) Proteoglycan arrays in the cochlear basement membrane. Hear Res 157:65–76